ACCOUNTS
—of materials research—

pubs.acs.org/amrcda

Article

Element-Resolved Imaging of Electrochemical Materials with X-ray Fluorescence Microscopy

Yetong Jia, Dawei Xia,* Changlian Wen, Feng Lin, Kejie Zhao,* and Luxi Li*

Cite This: *Acc. Mater. Res.* 2026, 7, 860−870

Read Online

ACCESS | Metrics & More | Article Recommendations

CONSPECTUS: Electrochemical systems feature complex and spatially heterogeneous elemental distributions that evolve during operation. Revealing these elemental dynamics is critical to understanding operation and degradation mechanisms, and thus to improving energy storage and conversion systems. X-ray fluorescence microscopy (XFM) provides a powerful, nondestructive, and element-specific probe for mapping elemental distributions with spatial resolution across relevant length scales. These capabilities enable XFM to address key questions in electrochemical materials research, including materials synthesis and compositional engineering, post-mortem analysis of aged materials, and operando visualization of elemental redistribution during electrochemical processes.

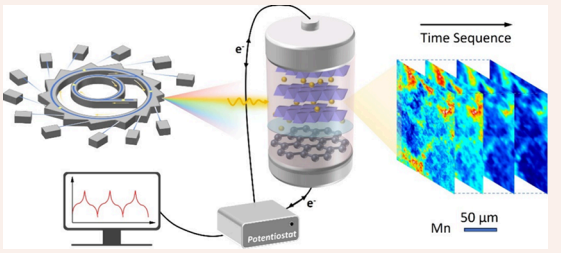

In this Account, we first introduce the mechanics and experimental setup of XFM, followed by its major capabilities and applications in electrochemical systems. We highlight its element specificity, high sensitivity, multielement detection, penetration power, and compatibility with operando and nondestructive measurements, which together make it suitable for probing complex and spatially heterogeneous electrochemical materials. We also compare XFM with other elemental analysis techniques to clarify its distinctive advantages. We then summarize ex situ XFM studies of electrochemical materials. In materials design and compositional engineering, XFM can directly verify whether intended elemental architectures are successfully realized, including surface coatings, elemental doping, and concentration-gradient designs in battery electrodes. This capability is important because the performance of engineered materials often depends not only on the presence of specific elements but also on their spatial distribution. In postcycling analysis, XFM reveals unintended elemental redistribution associated with degradation, such as transition-metal dissolution and deposition, polysulfide migration, electrolyte heterogeneity, and the formation of spatially localized reaction products or byproducts. These examples show how XFM connects elemental heterogeneity with electrochemical function and failure mechanisms. We further highlight operando and in situ XFM studies that directly visualize dynamic elemental evolution in working electrochemical systems. These studies are discussed in two categories: elemental evolution within bulk electrochemical materials and interfacial processes at electrode−electrolyte interfaces. By repeatedly probing the same region during operation, XFM can track dynamic electrochemical phenomena such as dissolution−redeposition, reversible and irreversible phase evolution, and elemental diffusion layers, which are difficult to reconstruct from post-mortem analysis alone. Dynamic behavior captured by XFM enables the correlation of spatial, temporal, and compositional information with electrochemical performance.

Following representative scientific case studies, we finally discuss the current limitations and future opportunities of XFM in electrochemical research. Although XFM directly links elemental distributions with electrochemical function and degradation, its broader application is still limited by trade-offs among spatial resolution, temporal resolution, sensitivity, and field of view, especially for high-resolution, three-dimensional, and operando measurements. Future advances in higher-brilliance synchrotron sources, faster scanning schemes, improved energy-dispersive detectors, focusing optics, positioning systems, multimodal integration, real-time data processing, quantitative reconstruction, and AI/ML-assisted analysis are expected to improve throughput, spatial and temporal resolution, quantitative interpretation, and the analysis of large XFM data sets. Looking forward, XFM is expected to be applied to broader electrochemical systems and to become an increasingly powerful tool for guiding the design and mechanistic understanding of next-generation electrochemical materials and devices.

1. INTRODUCTION

Electrochemical systems underpin modern technologies for energy storage, energy conversion, and adaptive functionality. Rechargeable batteries power portable electronics, electric vehicles, and grid-level storage,[1,2] while electrochromic devices such as smart windows enable dynamic control of light

Received: April 6, 2026
Revised: May 21, 2026
Accepted: June 21, 2026
Published: July 14, 2026

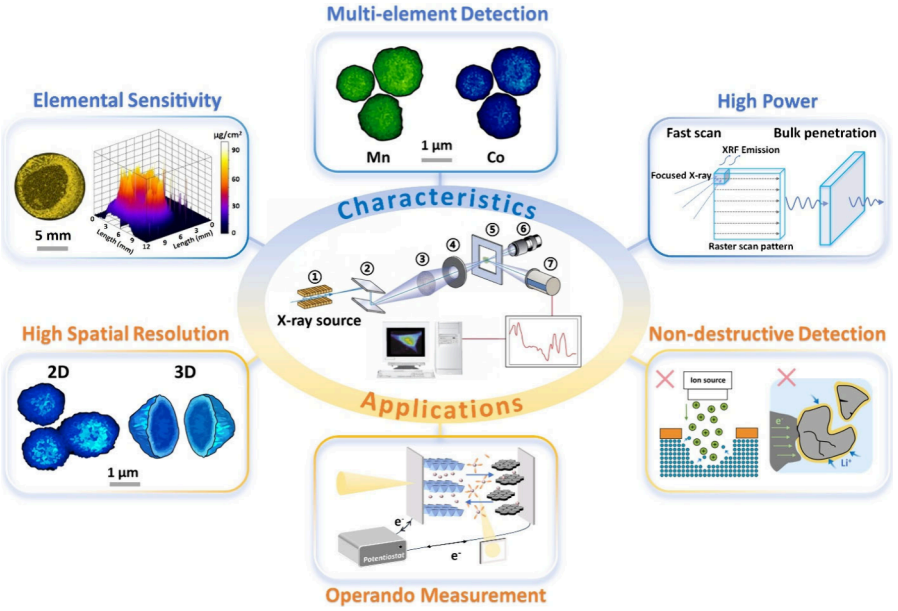

Figure 1. Characteristics and applications of XFM in analyzing electrochemical systems. XFM has unique characteristics including elemental sensitivity, multielement detection, and high power including both high flux and high energy. These characteristics enable high-spatial resolution, operando measurement, and nondestructive detection of XFM in electrochemical systems. ① to ⑦ in the XFM setup[15] are undulator, monochromator, Fresnel zoneplate, order-sorting aperture, specimen holder, transmission detector, and X-ray fluorescence detector. Reproduced with permission from ref 15. Copyright 2007 Elsevier Ltd.

transmission.[3,4] Fuel cells, electrolyzers, and electrocatalytic systems further support the interconversion of electricity and chemical fuels, expanding the role of electrochemistry in sustainable energy technologies.[5] Despite their diversity, these systems share common materials requirements, including high efficiency, durability, reversibility, reproducibility, and operational safety.[6,7] Understanding their performance and failure mechanisms is therefore critical for the rational design and development of advanced electrochemical materials.

Electrochemical performance and degradation are governed by coupled reactions and mass transport at the electrode−electrolyte interface.[8−11] During operation, elemental distributions in the electrode, electrolyte, and mobile species evolve continuously and often in a spatially heterogeneous manner. Such compositional evolution can strongly influence reaction pathways, reversibility, and long-term stability. In the classic electrochromic WO_3 system, in situ electrodeposition modifies the electrode−electrolyte interface and significantly improves electrochemical performance.[12] In mixed-metal hydroxide catalysts for the oxygen evolution reaction (OER), phase segregation and elemental redistribution can be reversible under operating conditions, highlighting the dynamic nature of catalyst evolution under electrochemical bias.[13] In rechargeable batteries, irreversible transition-metal dissolution during long-term cycling is closely associated with cathode degradation and performance decay.[14] These examples illustrate the importance of spatially resolved, element-specific characterization capable of tracking dynamic compositional evolution in electrochemical systems.

X-ray fluorescence microscopy (XFM) provides a direct link between elemental distributions and mechanistic studies in electrochemical systems. As a nondestructive and element-specific imaging method, XFM enables spatially resolved visualization of chemical elements in complex specimens.[15,16] Recent developments in operando XFM have further enabled spatially and temporally resolved analysis of elemental evolution during electrochemical reactions.[17] These capabilities make XFM well suited for examining materials synthesis and compositional engineering,[18−20] as well as for tracking elemental redistribution in working electrodes. In particular, operando XFM can directly visualize dissolution and redeposition of electrode species, providing mechanistic insight into interfacial evolution during electrochemical operation. The simultaneous detection of multiple elements further enables correlated analysis of interacting interfacial species and their coupled evolution during operation.[21,22]

In this Account, we first introduce the fundamental principles of XFM and highlight the features that make it particularly suitable for electrochemical studies.[15−17,23] We then review ex situ XFM studies of electrochemical materials, focusing on applications in materials design and compositional engineering as well as postcycling analysis of degradation and failure.[14,18−20,24,25] Next, we discuss operando and in situ XFM studies, emphasizing both elemental redistribution in bulk electrode materials and dynamic processes at electrode−electrolyte interfaces.[12,13,17,21,22,26,27] Finally, we examine current limitations of XFM in electrochemical research, particularly the trade-offs among spatial resolution, temporal resolution, and experimental complexity, and provide an outlook on future opportunities in faster imaging, multimodal characterization, and next-generation electrochemical XFM platforms.

2. PRINCIPLES AND CAPABILITIES OF XFM

X-ray fluorescence occurs when an inner-shell electron is ionized from an atom and the resulting vacancy is then filled by an outer-shell electron to stabilize the atom, while an X-ray photon is emitted.[16] The energy of the emitted X-ray photon is equal to the difference in binding energies of the two electronic states and serves as the fingerprint of the chemical element. The intensity of the fluorescent photons is then used for elemental quantification. XFM is a scanning-probe microscopy technique based on the X-ray fluorescence phenomenon. In a typical XFM

https://doi.org/10.1021/accountsmr.6c00091
Acc. Mater. Res. 2026, 7, 860−870

experiment, a monochromatized X-ray beam is focused onto the specimen and raster-scanned across the sample. The fluorescent photons are measured by an energy-dispersive detector to generate spatially resolved elemental maps. Figure 1 illustrates the setup of a synchrotron XFM microscope and highlights its unique capabilities and feasibility for analyzing electrochemical systems.

XFM is an element-specific technique that provides spatially resolved elemental distributions in specimens. The optimal resolution of the instrument is defined by the X-ray spot size. Under optimized hard X-ray nanoprobe conditions, spatial resolutions approaching ~10 nm[28] have been demonstrated at advanced beamlines. The energy-dispersive detector enables simultaneous detection of multiple elements. XFM also offers high sensitivity and can detect elements at sub-ppm concentrations. Because hard X-rays have strong penetration power, XFM is a nondestructive method for probing elemental distributions in complex specimens and buried structures. In addition to conventional two-dimensional mapping, XFM can be extended to three-dimensional analysis through XFM tomography for bulk-like samples,[29] confocal XFM, and more recently XFM laminography both for planar specimens.[30] Despite their different experimental configurations, these approaches remain time-consuming because of their scanning-probe nature and stringent demands on sample stability, mechanical precision, and data processing.

Synchrotron radiation provides a high-brilliance X-ray beam with tunable energy, enabling focused X-ray probes, fast scanning, and operando compatibility. These features are particularly important for electrochemical studies of dilute species, dynamic elemental redistribution, and buried interfaces. At the same time, the dependence on synchrotron facilities limits accessibility and experimental throughput.

Compared with other elemental analysis techniques, XFM provides a distinctive combination of high penetration power, nondestructive probing, multielement detection, and spatially resolved imaging. Scanning electron microscopy-energy dispersive X-ray spectroscopy (SEM-EDX) is widely used for elemental mapping, but it is mainly sensitive to near-surface regions and is less suitable for probing buried materials or complex electrochemical environments. X-ray photoelectron spectroscopy (XPS) is another surface-sensitive and semi-quantitative technique for measuring elemental composition, and recent developments have enabled elemental mapping with micrometer-scale spatial resolution.[31] Hand-held XFM instruments are commonly used for bulk elemental analysis of macroscopic specimens, but they do not provide the spatial resolution required for studying microscale heterogeneity, for example, <10 μm. For precise bulk quantification of elemental composition, inductively coupled plasma mass spectrometry (ICP-MS) is widely used; however, it is a destructive technique and lacks spatial information. Thus, the key advantage of XFM is not any single capability alone, but the integration of high penetration depth, nondestructive probing, multielement detection, and spatially resolved imaging in one technique.

3. EX SITU XFM STUDIES OF ELECTROCHEMICAL MATERIALS

3.1. Material Design and Engineering

Electrochemical materials are often improved through elaborate compositional and surface engineering rather than solely through the discovery of new compounds. Common strategies include surface coating, elemental doping, and concentration-gradient design, all of which aim to enhance structural stability, suppress parasitic reactions, mitigate the loss of redox active elements, and improve long-term electrochemical performance.[14,27,32] Because the effectiveness of these approaches depends not only on composition but also on spatial distribution, characterization methods that directly resolve elemental heterogeneity are essential for verifying whether the intended material architecture is realized. XFM provides a nondestructive means to map two-dimensional and three-dimensional elemental distributions across multiple length scales, from whole electrodes (millimeter scale) to individual secondary and primary particles (micrometer scale). As a result, XFM is particularly well suited for evaluating the quality of engineered electrochemical materials and for linking spatial compositional design to electrochemical function. Figure 2 highlights representative applications of XFM in the inspection of micro-engineered electrode materials.

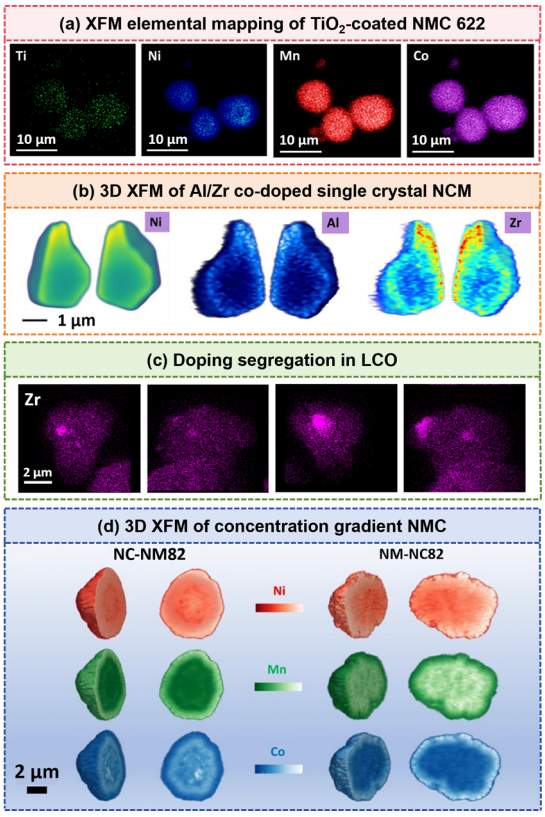

Figure 2. XFM mapping of microengineered cathode materials for rechargeable batteries. NMC is a leading layered oxide family for lithium-ion batteries, generally expressed as $LiNi_xMn_yCo_zO_2$ ($x + y + z = 1$). (a) 2D XFM elemental maps for a TiO_2-coated NMC622 cathode.[18] Reproduced with permission from ref 18. Copyright 2018 American Chemical Society. (b) 3D XFM tomography of a single-crystal Ni-rich NMC particle codoped with Al and Zr. Al is found throughout the crystal indicating uniform lattice doping, whereas Zr is enriched at the particle surface with a segregated dopant layer.[19] Reproduced with permission from ref 19. Licensed under a Creative Commons Attribution 4.0 International License. (c) An unsuccessful doping case in one $LiCoO_2$ (LCO) cathode particle from different projections, where the Zr dopant segregated into localized regions instead of uniformly dispersed. (d) 3D XFM tomography of concentration-gradient cathode particles, showing two particles of different Mn and Co concentration from the core toward the surface with Ni relatively uniform to investigate the correlation between hierarchical composition design and mechanical stability.[20] Reproduced with permission from ref 20. Licensed under a Creative Commons Attribution 4.0 International License.

https://doi.org/10.1021/accountsmr.6c00091
Acc. Mater. Res. 2026, 7, 860−870

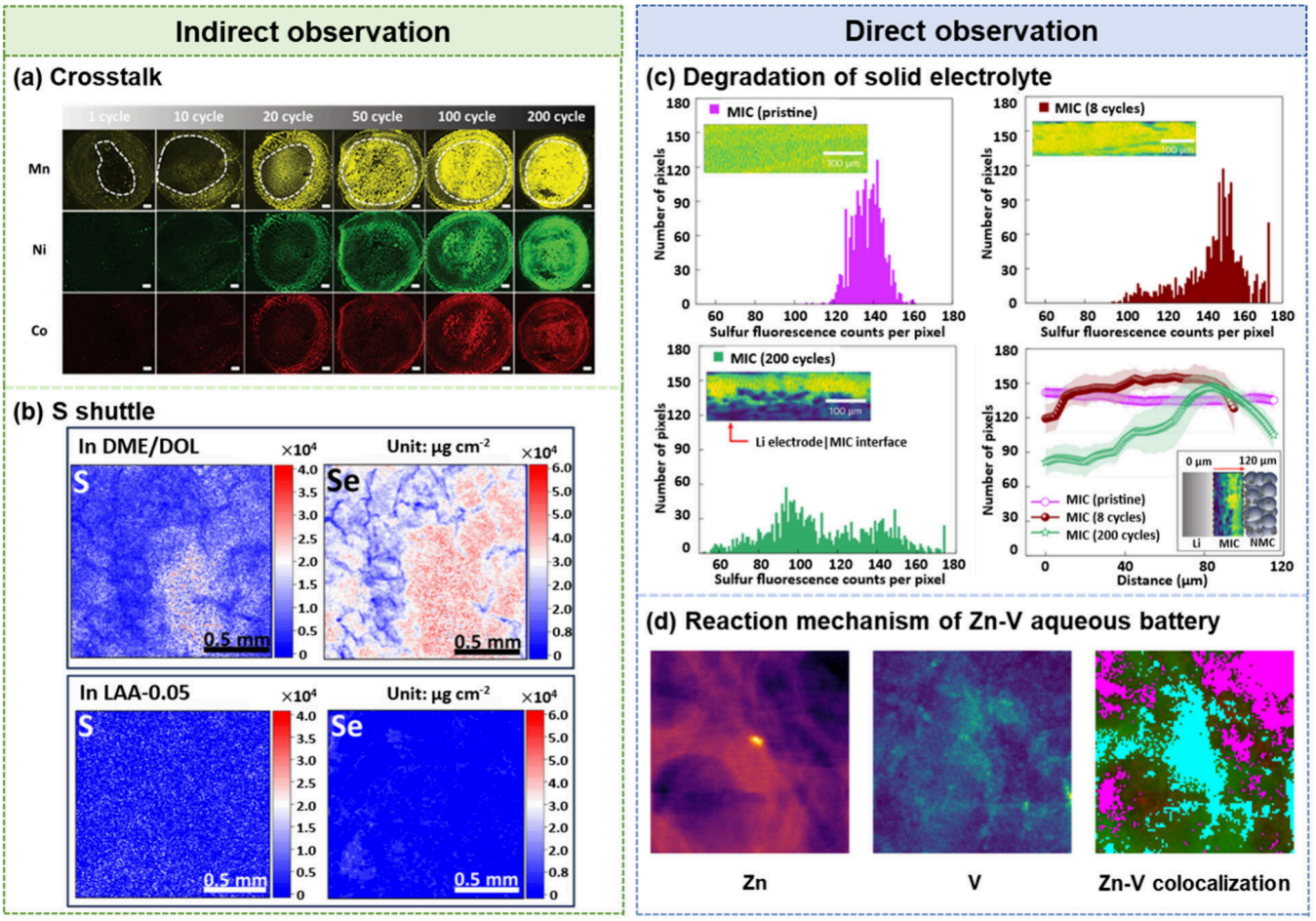

Figure 3. Ex situ XFM data of electrodes or electrolytes after cycling. (a) XFM maps of Mn, Co and Ni element on Li metal anodes, which quantify transition metal deposition at constant charging rate 1C after different cycles. The scale bars are 1 mm.[14] Reproduced with permission from ref 14. Copyright 2023 Wiley-VCH GmbH. (b) XFM maps of S and Se elements on Li metal anodes of Li−S battery after cycling in two different electrolytes (1,2-dimethoxyethane, DME/1,3-dioxolane, DOL) with and without Lewis acid additive (LAA). The color bar indicates the signal intensity changing from blue (low) to red (high).[38] Reproduced with permission from ref 38. Copyright 2024 Elsevier Inc. (c) XFM maps and diagrams of sulfur in MIC electrolyte before and after cycling, which indicate local depletion of mobile ionic liquid and ionic concentration heterogeneity of MIC reclaimed from Li||NMC811 cell configuration. In the color bar, bright yellow pixels indicate a higher concentration of sulfur species while dimmer green pixels present a lower concentration. Scale bars are all 100 μm. The diagram shows the sulfur concentration throughout MIC electrolyte.[8] Reproduced with permission from ref 8. Copyright 2025 Springer Nature. (d) XFM map and correlation map of Zn and V element on discharged V_2O_5 cathode in Zn|| V_2O_5 aqueous battery. Dimension: 0.2 mm. Bright color indicates higher element concentration for Zn and V maps. The right marked map reflects the Zn/V colocalization relationship: the cyan color represents the top 20% of colocalization and magenta color represents bottom 20% colocalization.

Surface coating is a widely used engineering strategy for stabilizing electrochemical interfaces. Oxides, phosphates, polymers, and other chemically stable compounds can serve as artificial passivation layers between the active material and the liquid electrolyte.[33−35] Such coatings can alleviate transition-metal dissolution and irreversible phase transition during cycling.[36,18] Because their effectiveness depends strongly on thickness and spatial uniformity, direct elemental mapping is important for evaluating coating quality. XFM is particularly useful in this context because it can nondestructively confirm the presence and distribution of coating elements. For example, Gao et al.[18] applied TiO_2 coating to $LiNi_{0.6}Mn_{0.2}Co_{0.2}O_2$ (NMC622) secondary particles to improve the high-voltage cycling stability. As shown in Figure 2(a), the Ti map reveals a uniform Ti distribution across the particles, confirming the successful formation of a Ti-based surface coating layer on NMC622. This result illustrates how XFM can directly verify whether a surface coating strategy is spatially realized as intended.

Elemental doping is another important materials-engineering strategy for improving the structural and chemical stability of cathodes. In this approach, a small fraction (i.e., <10 wt %) of the host elements is replaced by foreign dopants, often metal cations such as Mg, Al, Ti, or Zr.[34,37] The spatial distribution of these dopants is critical, because their benefits depend not only on composition but also on whether they are incorporated uniformly, enriched near the surface, or segregated into localized regions. XFM is particularly effective for evaluating such dopant distributions through direct elemental mapping. For example, Ou et al.[19] improved Ni-rich cathode materials using Al/Zr codoping. In this design, Al enhances Li-ion mobility, relieves internal strain, and suppresses Li/Ni cation mixing during high-voltage cycling, while a Zr-enriched outer region promotes the formation of a more stable cathode−electrolyte interphase and suppresses interfacial degradation. As shown in Figure 2(b), three-dimensional XFM tomography of a single-crystal Ni-rich NMC particle reveals strong colocalization of Al, Zr, and Ni, consistent with successful dopant incorporation. In contrast, Figure 2(c) shows nonuniform Zr distribution in a Zr-doped $LiCoO_2$ single particle, where the dopant segregates into localized regions rather than remaining spatially homogeneous. These examples demonstrate that XFM can distinguish between successful and nonideal doping outcomes, providing direct feedback for optimizing compositional engineering strategies.

Beyond adding foreign elements through doping or coating, concentration-gradient design offers another strategy for engineering cathode materials by spatially varying the distribution of native

https://doi.org/10.1021/accountsmr.6c00091
Acc. Mater. Res. 2026, 7, 860−870

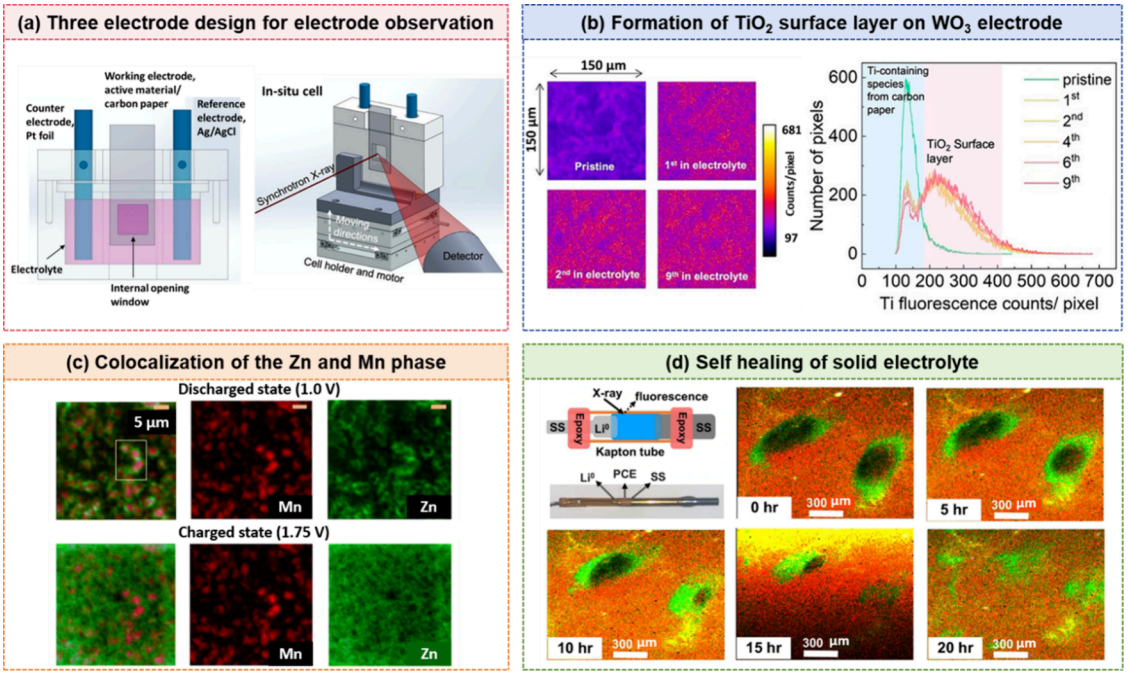

Figure 4. In situ XFM for bulk detection in electrochemical systems. (a) Schematic of an operando XFM cell design for electrode bulk observation.[12] Reproduced with permission from ref 12. Copyright 2022 American Chemical Society. (b) Formation and quantification of a surface layer on a WO_3 electrode revealed by operando XFM. XFM map of Ti element showing progressive signal buildup after cycles, consistent with deposition of a solid TiO_2 layer on the WO_3 matrix. Quantitative Ti distribution over cycles is depicted on the right line graph.[12] Reproduced with permission from ref 12. Copyright 2022 American Chemical Society. (c) Operando XFM maps for aqueous Zn||MnO_2 cell showing Mn (red) and Zn (green) elements, and the overlay Zn/Mn element maps. The above and below maps correspond to discharged (1.0 V) and charged (1.75 V) states of the MnO_2 electrode, respectively. The scale bars are all 5 μm.[26] Reproduced with permission from ref 26. Copyright 2023 The Royal Society of Chemistry. (d) Schematic illustration of the tube battery and operando XFM maps of S (green) and P (red) for a self-healing plastic-ceramic electrolyte revealing the closure of a void over time. Li metal is set as the reference electrode and stainless steel (SS) as the working electrode.[48] Reproduced with permission from ref 48. Licensed under a Creative Commons Attribution 4.0 International License.

transition metals within individual particles. In battery cathodes such as NMC, this approach aims to exploit the distinct functions of Ni, Co, and Mn by placing each element where it is most beneficial. XFM is particularly valuable for this type of materials design because it can directly visualize three-dimensional elemental architectures that cannot be verified from bulk composition alone. For example, Figure 2(d) shows 3D XFM tomography of two concentration-gradient NMC811 particles.[20] One particle features a Co-enriched shell and Mn-enriched core, whereas the other has a Mn-enriched shell and Co-enriched core; in both cases, the Ni distribution remains relatively uniform with depth. These distinct concentration gradients lead to markedly different electrochemical and mechanical behaviors. The Co-rich-shell/Mn-rich-core particle exhibits improved morphological stability and slower capacity fade without sacrificing capacity, whereas the opposite architecture results in more severe particle cracking and poorer rate performance. This example highlights how XFM can directly verify concentration-gradient architecture and guide the rational tuning of spatial-compositional design in electrochemical materials.

3.2. Postcycling and Degradation Analysis

Whereas ex situ XFM of engineered materials is mainly used to verify intended compositional architectures in pristine electrodes, postcycling ex situ XFM reveals unintended elemental redistribution that develops during electrochemical operation. This capability is particularly valuable because many degradation pathways in electrochemical systems are fundamentally spatial redistribution problems: active elements dissolve, migrate, redeposit, or accumulate in locations different from where they originated. By mapping elemental distributions after cycling and quantifying pixelwise correlations among multiple elements, ex situ XFM can provide mechanistic insight that is difficult to obtain from bulk electrochemical measurements alone. As illustrated in Figure 3, postcycling XFM can be broadly divided into indirect and direct observation. In indirect observation, the scanned component is not the original source of the redistributed species, but rather the location where those species ultimately accumulate. In direct observation, XFM probes the cycled electrode or electrolyte itself to resolve spatial changes in active species, reaction products, or byproducts.

A representative example of indirect observation is transition-metal cathode-to-anode crosstalk in rechargeable batteries. Transition-metal dissolution originates at the cathode−electrolyte interface, where the quantity depends strongly on electrolyte chemistry and operating conditions.[9] The dissolved transition metals then migrate through the electrolyte and deposit on the counter electrode, where they can be quantified sensitively by XFM. This process has been reported for nearly all major cathode families, including NMC, $LiCoO_2$, $LiMn_2O_4$, and $LiFePO_4$,[25,39,40] and even trace deposition (ppm level) onto the anode surface can cause capacity decay.[41−43] Figure 3(a) shows XFM maps of Mn, Ni, and Co deposited on Li metal anodes after different numbers reclaimed from cells using Li-rich layered oxide $Li_{1.2}Ni_{0.13}Co_{0.13}Mn_{0.54}O_2$ as the cathode.[14] The intensities of all three elements increase progressively with cycle number, consistent with continuous transition-metal dissolution from the cathode and cumulative deposition on the Li metal anode. In addition, the spatial distributions of Mn, Ni, and Co on the Li surface are broadly similar, suggesting that the deposition pattern is influenced by common factors such as local surface roughness or pressure distribution. These results illustrate how postcycling XFM can convert crosstalk into a directly mappable spatial signature of degradation.

A similar logic applies to other dissolved-species migration processes, such as the sulfur shuttle in Li−S batteries. In these systems, sulfur undergoes a multistep conversion from solid sulfur to soluble lithium polysulfides and finally to solid Li_2S during discharge.[44] Intermediate polysulfides can migrate from the cathode to the Li metal anode and redeposit there, leading to active-material loss at the cathode and

https://doi.org/10.1021/accountsmr.6c00091
Acc. Mater. Res. 2026, 7, 860−870

parasitic degradation at the anode.[45,46] Figure 3(b) demonstrates how ex situ XFM can evaluate the effectiveness of electrolyte engineering in suppressing this process.[38] In that study, selenium (Se) was introduced into the sulfur cathode to improve electronic conductivity, but the dissolved Se-containing species also migrated and deposited with the polysulfides. When the Lewis acid additive $LiBF_4$ was added to the electrolyte, both S and Se deposition on the Li metal anode were markedly suppressed judged from the XFM maps, in agreement with the improved cycling and rate performance. Together with transition-metal crosstalk, this example shows that ex situ XFM is effective for quantifying migrated species that originate at one electrode but accumulate at another, thereby linking quantity or spatial heterogeneity of deposited elements to degree of battery degradation.

Postcycling XFM can also provide direct observation of elemental redistribution within cycled electrolytes and electrodes themselves. One example is the molecular ionic composite (MIC) electrolyte, which consists of a rigid poly-2,2′-disulfonyl-4,4′-benzidine terephthalamide (PBDT) framework and an ionic liquid phase that provides ionic conductivity.[8] Figure 3(c) shows cross-sectional XFM maps of sulfur species in the MIC electrolyte before and after cycling. Whereas the pristine electrolyte exhibits a nearly uniform sulfur distribution, cycling leads to pronounced sulfur depletion especially near the Li metal/electrolyte interface, reflecting depletion of ionic liquid associated with unstable interphase formation and decomposition of the PBDT host. This interfacial heterogeneity aligns with increased cell impedance, poor Li metal reversibility, and reduced critical current density of symmetric Li metal cells. Direct postcycling XFM mapping can likewise reveal reaction products and side reactions in electrodes. In a rechargeable Zn||V_2O_5 aqueous battery, for example, Zn^{2+} and H^+ cointercalation during discharge forms protonated vanadium bronze phases, while the local pH increase also drives formation of the insulating byproduct zinc hydroxy sulfate (ZHS).[21,47] As shown in Figure 3(d), XFM maps and Zn−V colocalization analysis of the discharged V_2O_5 cathode distinguish Zn associated with vanadium-host intercalation from Zn associated with ZHS deposits surrounding cathode agglomerates.[26] This spatial separation clarifies the reaction mechanism, confirms the existence of the byproduct phase, and highlights the need to control ZHS formation. To summarize, these studies show that ex situ XFM is not limited to locating redox-active species after cycling; it can also help elucidate electrolyte changes arising from bidirectional electrode−electrolyte interactions.

4. OPERANDO AND IN SITU XFM STUDIES

4.1. Dynamics of Elemental Distribution in Bulk Electrochemical Materials

In contrast to ex situ analysis, in situ and operando XFM repeatedly probe the same region of a working electrochemical system and directly track the spatiotemporal evolution of elemental distributions during operation. For both electrode materials and electrolytes, this capability is especially valuable because it reveals transient redistribution, reversibility of solid−liquid conversion, and divergent reaction pathways that are often difficult to infer reliably from post-mortem measurements alone. Figure 4(a) shows a representative in situ electrochemical cell design for bulk observation.[12] In this three-electrode configuration, the working electrode is positioned toward the incident X-ray beam, while the counter and reference electrodes are placed on the sides, allowing repeated X-ray interrogation of the same electrode region under applied bias.

Hu et al. used this in situ configuration to investigate the dynamic modification of WO_3 electrochromic electrodes during repeated proton insertion and extraction.[12] In principle, proton intercalation in WO_3 reversibly changes the optical state of the electrode from transparent to blue. However, repeated cycling in sulfuric acid induces nonfaradaic dissolution−redeposition of WO_3, which contributes to device degradation over time. The presence of Ti (IV), either introduced as an electrolyte additive or released from surface coatings, was found to improve the durability of the WO_3 electrode. As shown in Figure 4(b), in situ XFM directly visualizes the progressive formation of an amorphous TiO_2 surface layer on WO_3 from Ti-containing electrolytes. The shift of element-count histograms toward higher Ti fluorescence intensities with cycling indicates continuous layer buildup across the porous film. This operando elemental mapping correlates with improved Coulombic efficiency and enhanced optical modulation, demonstrating how in situ XFM can reveal constructive dissolution−redeposition processes which dictates reaction reversibility.

Operando XFM has also provided direct evidence for reaction pathways in battery electrodes, helping resolve long-standing mechanistic questions in systems such as aqueous Zn||MnO_2 batteries. A range of charge storage mechanisms has been proposed for MnO_2 cathodes, including Zn^{2+} insertion/extraction, H^+/Zn^{2+} coinsertion, conversion reactions, and dissolution−deposition.[26,49−51] In situ XFM offers a direct means to distinguish among these possibilities by visualizing the evolution of Mn- and Zn-containing phases during cycling. Figure 4(c) shows XFM maps of Mn and Zn in the MnO_2 electrode during the third cycle.[26] In the discharged state, Zn and Mn maps indicate high colocalization of Zn-rich phase and MnO_2, which was attributed to the zinc hydroxy sulfate (ZHS) precipitation rather than Zn-ion intercalation. Such high spatial affinity corroborates the pH-modulating role of ZHS as a consequence of local proton consumption. Upon subsequent charging, this colocalization largely disappears, indicating the reversibility of the ZHS phase and the formation of other Zn-rich phases. Combined with complementary synchrotron techniques, these measurements support an electrodissolution−electrodeposition mechanism with ZHS-mediated pH modulation.[26,52] These results highlight how operando XFM can disentangle dynamic bulk reaction pathways in multi-material systems.

Beyond electrode−electrolyte reactions, in situ XFM can also probe the dynamic evolution of electrolytes alone. A tube-cell configuration is shown in Figure 4(d).[48] This design was used to investigate a plastic ceramic electrolyte composed of $Li_{1.5}Al_{0.5}Ti_{1.5}(PO_4)_3$ (LATP) particles embedded in a self-healing solid polymer electrolyte with a dynamic bonding network. P and S served as elemental markers for the LATP ceramic and polymer phases, respectively. XFM maps reveal the healing kinetics of initially voided regions: the sulfur-containing polymer phase first infiltrates the voids because of its dynamically cross-linked nature, followed by migration of micron-sized LATP particles through the matrix to further fill the defects. This example shows that in situ XFM is not limited to following redox-active electrode species; it can also spatiotemporally resolve chemo-mechanical evolution in bulk solid electrolytes, providing insight into defect healing and structural stabilization in next-generation solid-state systems.

4.2. Interfacial Processes at Electrode−Electrolyte Interfaces

Directly visualizing the electrode−electrolyte interface across relevant length scales is essential for understanding and engineering electrochemical systems with improved durability and faster kinetics. Because many of the most important processes in electrochemistry occur within buried interfacial regions, specialized in situ XFM geometries have been developed to directly probe these interfaces during operation.

https://doi.org/10.1021/accountsmr.6c00091
Acc. Mater. Res. 2026, 7, 860−870

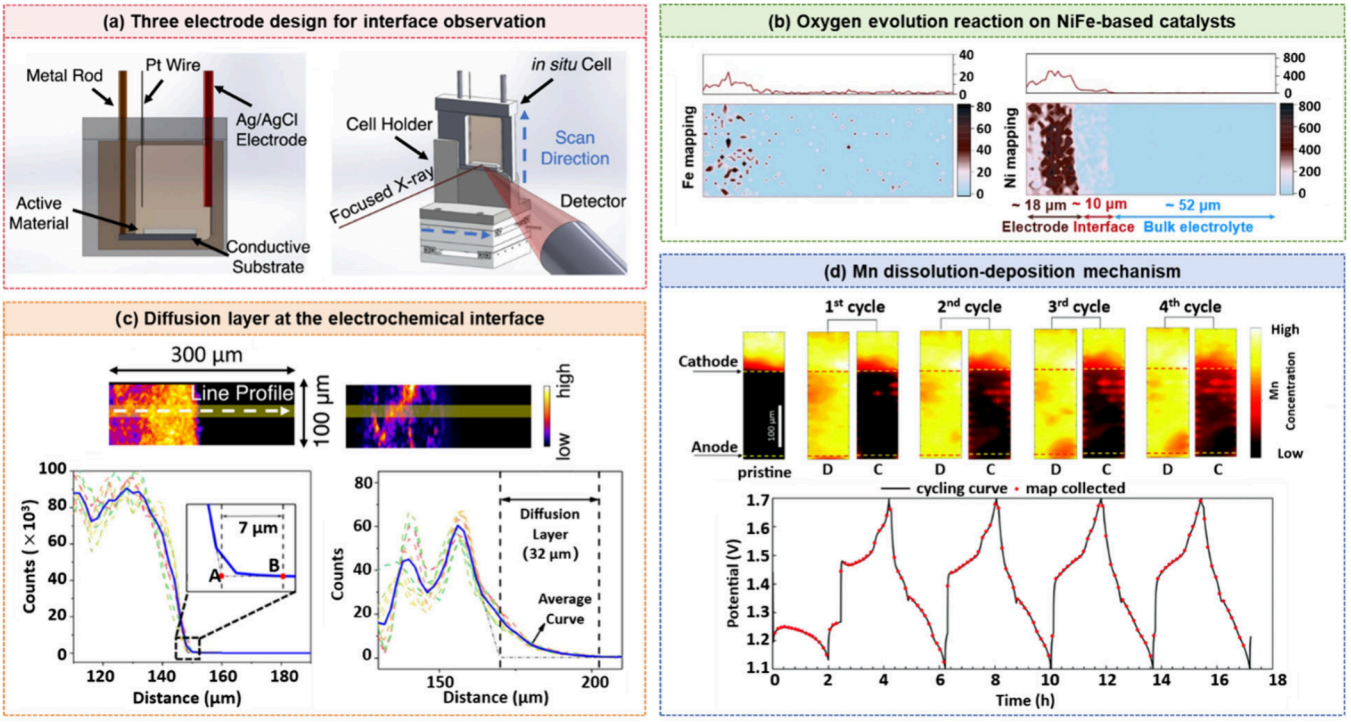

Figure 5. In situ XFM for interface detection in electrochemical systems. (a) Schematic of an operando XFM cell design for electrode−electrolyte interface observation.[17] Reproduced with permission from ref 17. Copyright 2022 The Electrochemical Society. (b) Operando XFM maps showing the fluorescence intensity distribution of Fe (left) and Ni (right) ions from the NiFe-based catalyst electrode region to the bulk electrolyte region at 1.63 V versus RHE. The curve above each XFM map shows the fluorescence intensity distribution from the electrode to the electrolyte. The color scale indicates the fluorescence intensity, which has the unit of fluorescence counts per pixel.[22] Reproduced with permission from ref 22. Copyright 2025 Springer Nature. (c) Evolution of a dissolution-induced diffusion layer above a Mn-based cathode before (left) and after adding electrolyte (right). The left XFM map is at the solid−air interface without adding electrolyte and has a sharp interface. The right XFM map is after injecting electrolyte and shows a broadened diffusion layer. The below line profiles are intensities calculated from the yellow shaded area in the zoomed-in region around the electrode interface.[17] Reproduced with permission from ref 17. Copyright 2022 The Electrochemical Society. (d) Operando Mn XFM maps from MnO_2 cathode to aqueous electrolyte at fully discharged (D) and charged (C) states for the first four cycles. In the electrolyte, the Mn intensity is high in the fully discharged state of each cycle while it is low in the fully charged state. The curve below shows galvanostatic discharge and charge profiles during operando experiment with XFM maps collected at each red point.[21] Reproduced with permission from ref 21. Copyright 2020 The Royal Society of Chemistry.

In one common design, the cross-section of the working electrode is oriented perpendicular to the incident X-ray beam so that raster scanning spans from the electrode into the adjacent electrolyte. Figure 5(a) shows a customized three-electrode cell based on this concept, in which a thin-film working electrode is deposited on a conductive substrate.[17] This configuration exposes the buried solid−liquid interface, provides spatial coverage from the electrode into the bulk electrolyte, and minimizes interference from the counter electrode and other cell components. Repeated scanning across the same interfacial region then enables direct visualization of elemental distributions and their evolution under operando conditions.

In situ interfacial XFM is particularly powerful for resolving diffusion layers and dynamic species exchange between electrodes and electrolytes. One representative example is the oxygen evolution reaction on NiFe-based electrocatalysts. Figure 5(b) shows the fluorescence intensity distributions of Fe and Ni extending from the catalyst surface into the bulk electrolyte.[22] Both elements exhibit interfacial diffusion layers under dissolution−redeposition equilibrium. Combined with complementary spectroscopies and electrochemical quartz-crystal microbalance measurements, the XFM results revealed a cooperative solid−molecular mechanism in which dissolved FeO_4^{2-} acts as a mobile cocatalyst that shuttles oxygen intermediates between solution and solid NiFe sites. This dynamic exchange between dissolved and surface-associated species enables catalytic behavior beyond the conventional scaling constraints of single-site surface mechanisms. More broadly, this study shows that in situ interfacial XFM can directly visualize catalyst-interface chemistry and elemental redistribution processes that govern electrocatalytic activity.

A similar approach has helped resolve interfacial reaction pathways in aqueous Zn||MnO_2 batteries as shown in Figure 5(d).[21] The Mn fluorescence intensity in the electrolyte is consistently higher in the discharged state and lower in the charged state. When current is applied, the fluorescence intensity increases in direct relation to discharge, whereas it changes only minimally during the rest period. These visualization and quantification therefore support the dissolution−deposition mechanism at the electrode scale and illustrate how in situ XFM can distinguish dynamic interfacial exchange processes that would be difficult to infer from ex situ measurements alone.

In situ interfacial XFM can also directly track the formation and evolution of diffusion layers associated with transition-metal dissolution. Figure 5(c) shows Mn maps recorded across the interface of a $LiMn_2O_4$ electrode before and after electrolyte addition.[17] Without electrolyte, the Mn signal changes sharply at the solid−air boundary. After electrolyte injection, the Mn profile broadens into the solution, indicating the formation of an

https://doi.org/10.1021/accountsmr.6c00091
Acc. Mater. Res. 2026, 7, 860−870

interfacial dissolution diffusion layer. Line profiles extracted near the interface further quantify this spatial broadening caused by chemical dissolution. Additional operando measurements showed that the Mn diffusion layer continued to evolve during cycling and approached a quasi-equilibrium thickness under modest applied bias. These results highlight the ability of interfacial XFM to capture both the emergence and steady-state behavior of dissolved transition-metal species near electrochemical interfaces.

Taken together, these studies demonstrate that in situ interfacial XFM provides an invaluable direct view of buried solid−liquid interfaces in working electrochemical systems, which is especially important for understanding bidirectional electrode−electrolyte interactions and for guiding the interface design toward more durable and efficient electrochemical devices.

5. CONCLUSION AND OUTLOOK

XFM has become an enabling platform for studying electrochemical materials because it directly links elemental distributions with electrochemical function and degradation. As highlighted in this Account, XFM has been applied to a broad range of electrochemical questions, from verifying engineered compositional architectures in pristine materials and identifying postcycling elemental redistribution, to directly visualizing dynamic processes in working electrodes and at buried electrode−electrolyte interfaces. Its combination of element specificity, high sensitivity, multielement detection, and penetration power makes it particularly well suited for probing chemically complex and spatially heterogeneous systems across relevant length scales.

Several practical constraints should be considered when applying XFM to electrochemical systems. First, conventional hard X-ray XFM is typically limited to elements with $Z \geq 13$, because fluorescence from lighter elements has low yield and is strongly attenuated by air, detector windows, electrolytes, and cell components. Second, XFM provides elemental rather than chemical-state contrast. Energy-dispersive detectors can separate fluorescence lines from different elements, but their energy resolution is generally insufficient to resolve oxidation states or local bonding environments. Third, XFM is a scanning-probe technique, so acquisition time is governed by pixel number, dwell time, fluorescence yield, and required signal-to-noise ratio. Operando measurements therefore require stable samples, beam intensity, positioning systems, and cell geometries. Finally, because pixels are collected sequentially, each map contains an intrinsic intraframe time delay, which can affect interpretation when the electrochemical process evolves on a time scale comparable to the scan time. These constraints require balancing elemental sensitivity, spatial resolution, field of view, temporal resolution, and measurement stability. Future advances in instrumentation and data analysis will further expand the capability of XFM. Higher-brilliance synchrotron sources, faster scanning schemes, improved detectors, focusing optics, and positioning systems will improve throughput, spatial resolution, and temporal resolution, especially for operando and three-dimensional measurements. Beyond conventional raster scanning, emerging full-field, multiplexed, and computational XFM approaches may provide alternative routes to faster elemental imaging and reduced temporal ambiguity within each image. For example, structured-illumination X-ray chemical imaging has recently integrated full-field transmission X-ray microscopy with XRF detection to recover nanoscale elemental maps without nanoscale beam focusing or point-by-point raster scanning.[53] Multimodal integration with micro-XRD, XANES, scattering, tomography, and electrochemical measurements will further connect elemental distributions with phase, structure, chemical state, and performance. As XFM data sets become larger and more multidimensional, AI/ML-assisted workflows will be increasingly important for spectral fitting, image registration, segmentation, feature tracking, correlation analysis, and adaptive scanning.

Although many current XFM studies in electrochemistry focus on battery materials, the method is broadly applicable to systems in which elemental redistribution, interfacial heterogeneity, and trace-species migration govern performance. In CO_2 reduction, XFM can help track catalyst restructuring, metal dissolution and redeposition, and local electrolyte or cation accumulation under bias. In fuel cells, it can visualize catalyst degradation, trace-metal migration, and catalyst-layer heterogeneity across membrane−electrode assemblies. In bioelectrochemical systems, XFM may provide spatially resolved information on metal centers, nutrient gradients, and interfacial reaction pathways associated with microbial electron transfer. As electrochemical materials become more compositionally complex and are increasingly studied under realistic operating conditions, XFM will play an important role in connecting spatially resolved elemental dynamics with mechanistic understanding and rational materials design. From a methodological perspective, XFM is most useful when the central scientific question involves spatial elemental redistribution rather than only average composition, especially when the target elements are medium- or high-Z species and when nondestructive or operando measurements are needed. Looking forward, the value of XFM in electrochemical research will continue to grow as the field moves toward more heterogeneous materials, more complex interfaces, and more realistic operando environments. Its unique ability to resolve spatially and temporally evolving elemental distributions makes it especially powerful for understanding how composition, transport, and reaction pathways are coupled in working systems. Together with continued developments in instrumentation, multimodal characterization, and data science, XFM is well positioned to play an increasingly important role in the design and mechanistic understanding of next-generation electrochemical materials and devices.

AUTHOR INFORMATION

Corresponding Authors

Dawei Xia − *Department of Chemistry, Virginia Tech, Blacksburg, Virginia 24061, United States;* orcid.org/0000-0003-4265-2528; Email: daweix20@vt.edu

Kejie Zhao − *School of Mechanical Engineering, Purdue University, West Lafayette, Indiana 47907, United States;* orcid.org/0000-0001-5030-7412; Email: kjzhao@purdue.edu

Luxi Li − *X-ray Science Division, Argonne National Laboratory, Lemont, Illinois 60439, United States*; Email: luxili@anl.gov

Authors

Yetong Jia − *School of Mechanical Engineering, Purdue University, West Lafayette, Indiana 47907, United States; X-ray Science Division, Argonne National Laboratory, Lemont, Illinois 60439, United States*

Changlian Wen − *School of Engineering, Brown University, Providence, Rhode Island 02912, United States*

https://doi.org/10.1021/accountsmr.6c00091
Acc. Mater. Res. 2026, 7, 860−870

Feng Lin − *Department of Chemistry, Virginia Tech, Blacksburg, Virginia 24061, United States; School of Engineering, Brown University, Providence, Rhode Island 02912, United States;* orcid.org/0000-0002-3729-3148

Complete contact information is available at: https://pubs.acs.org/10.1021/accountsmr.6c00091

Notes

The authors declare no competing financial interest.

Biographies

Yetong Jia is a Ph.D. student in Mechanical Engineering at Purdue University. Her research focuses on the degradation mechanism in electrochemical systems using multiscale modeling and the X-ray characterization method.

Dawei Xia is a postdoctoral researcher at Virginia Tech who received a Ph.D. degree in chemistry. He is dedicated to advancing next-generation energy storage based on earth-abundant elements.

Changlian Wen is pursuing his Ph.D. degree in Chemical and Environmental Engineering at Brown University. His research focuses on materials kinetics in energy storage systems.

Feng Lin is an associate professor of engineering at Brown University. His group focuses on materials electrochemistry for energy and sustainability, utilizing advanced synthesis and operando synchrotron characterization to design next-generation batteries, catalysts, and smart windows.

Kejie Zhao is a Professor of Mechanical Engineering and University Faculty Scholar at Purdue University. His group focuses on chemo-mechanics of electrochemically active materials using experimentation and multiscale modeling approaches.

Luxi Li is a Physicist and Beamline Scientist at Argonne National Laboratory. Her research focuses on the development and application of synchrotron X-ray techniques to investigate the electrochemical systems.

■ ACKNOWLEDGMENTS

L.L. and Y.J. acknowledge the support by the U.S. DOE Office of Science-Basic Energy Sciences, under Contract DE-SC0025702. This research used the beamline 2-ID-E of the Advanced Photon Source, a U.S. Department of Energy (DOE) Office of Science user facility operated for the DOE Office of Science by Argonne National Laboratory under Contract No. DE-AC02-06CH11357. K.Z. acknowledges the support by the National Science Foundation through grant DMR-2325463. D.X. and F.L. acknowledge the support from the Naval Enterprise Partnership Teaming with Universities for National Excellence (NEPTUNE), Office of Naval Research (Grant #N000142312609) and the Program Managers, Corey T. Love and Scott R. Higgins. W.C. and F.L. acknowledge the startup funds at Brown University.

■ REFERENCES

(1) Ngoy, K. R.; Lukong, V. T.; Yoro, K. O.; Makambo, J. B.; Chukwuati, N. C.; Ibegbulam, C.; Eterigho-Ikelegbe, O.; Ukoba, K.; Jen, T.-C. Lithium-ion batteries and the future of sustainable energy: A comprehensive review. *Renewable Sustainable Energy Rev.* **2025**, *223*, 115971.

(2) Goodenough, J. B.; Park, K. S. The Li-ion rechargeable battery: a perspective. *J. Am. Chem. Soc.* **2013**, *135* (4), 1167−1176.

(3) Gu, C.; Jia, A. B.; Zhang, Y. M.; Zhang, S. X. Emerging Electrochromic Materials and Devices for Future Displays. *Chem. Rev.* **2022**, *122* (18), 14679−14721.

(4) Wang, X.; Chen, K.; de Vasconcelos, L. S.; He, J.; Shin, Y. C.; Mei, J.; Zhao, K. Mechanical breathing in organic electrochromics. *Nat. Commun.* **2020**, *11* (1), 211.

(5) Zhang, W.; Hu, Y.; Ma, L.; Zhu, G.; Wang, Y.; Xue, X.; Chen, R.; Yang, S.; Jin, Z. Progress and Perspective of Electrocatalytic CO_2 Reduction for Renewable Carbonaceous Fuels and Chemicals. *Adv. Sci.* **2018**, *5* (1), 1700275.

(6) Chen, Y.; Kang, Y.; Zhao, Y.; Wang, L.; Liu, J.; Li, Y.; Liang, Z.; He, X.; Li, X.; Tavajohi, N.; Li, B. A review of lithium-ion battery safety concerns: The issues, strategies, and testing standards. *J. Energy Chem.* **2021**, *59* (8), 83−99.

(7) de Vasconcelos, L. S.; Xu, R.; Xu, Z.; Zhang, J.; Sharma, N.; Shah, S. R.; Han, J.; He, X.; Wu, X.; Sun, H.; Hu, S.; Perrin, M.; Wang, X.; Liu, Y.; Lin, F.; Cui, Y.; Zhao, K. Chemomechanics of Rechargeable Batteries: Status, Theories, and Perspectives. *Chem. Rev.* **2022**, *122* (15), 13043−13107.

(8) Min, J.; Bak, S.-M.; Zhang, Y.; Yuan, M.; Pietra, N. F.; Russell, J. A.; Deng, Z.; Xia, D.; Tao, L.; Du, Y.; Xiong, H.; Li, L.; Madsen, L. A.; Lin, F. Investigating the effect of heterogeneities across the electrode| multiphase polymer electrolyte interfaces in high-potential lithium batteries. *Nat. Nanotechnol.* **2025**, *20* (6), 787−797.

(9) Harris, O. C.; Lee, S. E.; Lees, C.; Tang, M. Review: mechanisms and consequences of chemical cross-talk in advanced Li-ion batteries. *J. Phys. Energy* **2020**, *2* (3), 032002.

(10) Dixit, M. B.; Park, J.-S.; Kenesei, P.; Almer, J.; Hatzell, K. B. Status and prospect of in situ and operando characterization of solid-state batteries. *Energy Environ. Sci.* **2021**, *14* (9), 4672−4711.

(11) Alsac, E. P.; Nelson, D. L.; Yoon, S. G.; Cavallaro, K. A.; Wang, C.; Sandoval, S. E.; Eze, U. D.; Jeong, W. J.; McDowell, M. T. Characterizing Electrode Materials and Interfaces in Solid-State Batteries. *Chem. Rev.* **2025**, *125* (4), 2009−2119.

(12) Hu, A.; Zhang, Y.; Yang, F.; Hwang, S.; Sainio, S.; Nordlund, D.; Maxey, E.; Dai, Q.; Gu, J.; Li, L.; Lin, F. Manipulating Interfacial Dissolution-Redeposition Dynamics to Resynthesize Electrode Surface Chemistry. *ACS Energy Lett.* **2022**, *7* (8), 2588−2594.

(13) Kuai, C.; Xu, Z.; Xi, C.; Hu, A.; Yang, Z.; Zhang, Y.; Sun, C.-J.; Li, L.; Sokaras, D.; Dong, C.; Qiao, S.-Z.; Du, X.-W.; Lin, F. Phase segregation reversibility in mixed-metal hydroxide water oxidation catalysts. *Nat. Catal.* **2020**, *3* (9), 743−753.

(14) Cao, B.; Li, T.; Zhao, W.; Yin, L.; Cao, H.; Chen, D.; Li, L.; Pan, F.; Zhang, M. Correlating Rate-Dependent Transition Metal Dissolution between Structure Degradation in Li-Rich Layered Oxides. *Small* **2023**, *19* (42), 2301834.

(15) Fahrni, C. J. Biological applications of X-ray fluorescence microscopy: exploring the subcellular topography and speciation of transition metals. *Curr. Opin. Chem. Biol.* **2007**, *11* (2), 121−127.

(16) Beckhoff, B.; Kanngießer, B.; Langhoff, N.; Wedell, R.; Wolff, H. *Handbook of Practical X-Ray Fluorescence Analysis*; Springer: Berlin, Germany, 2007.

(17) Zhang, Y.; Hu, A.; Maxey, E.; Li, L.; Lin, F. Spatiotemporal Visualization and Chemical Identification of the Metal Diffusion Layer at the Electrochemical Interface. *J. Electrochem. Soc.* **2022**, *169* (10), 100512.

(18) Gao, H.; Zeng, X.; Hu, Y.; Tileli, V.; Li, L.; Ren, Y.; Meng, X.; Maglia, F.; Lamp, P.; Kim, S.-J.; Amine, K.; Chen, Z. Modifying the Surface of a High-Voltage Lithium-Ion Cathode. *ACS Appl. Energy Mater.* **2018**, *1* (5), 2254−2260.

(19) Ou, X.; Liu, T.; Zhong, W.; Fan, X.; Guo, X.; Huang, X.; Cao, L.; Hu, J.; Zhang, B.; Chu, Y. S.; Hu, G.; Lin, Z.; Dahbi, M.; Alami, J.; Amine, K.; Yang, C.; Lu, J. Enabling high energy lithium metal batteries via single-crystal Ni-rich cathode material co-doping strategy. *Nat. Commun.* **2022**, *13* (1), 2319.

(20) Liu, T.; Yu, L.; Lu, J.; Zhou, T.; Huang, X.; Cai, Z.; Dai, A.; Gim, J.; Ren, Y.; Xiao, X.; Holt, M. V.; Chu, Y. S.; Arslan, I.; Wen, J.; Amine, K. Rational design of mechanically robust Ni-rich cathode materials via concentration gradient strategy. *Nat. Commun.* **2021**, *12* (1), 6024.

(21) Wu, D.; Housel, L. M.; Kim, S. J.; Sadique, N.; Quilty, C. D.; Wu, L.; Tappero, R.; Nicholas, S. L.; Ehrlich, S.; Zhu, Y.; Marschilok, A. C.; Takeuchi, E. S.; Bock, D. C.; Takeuchi, K. J. Quantitative temporally and spatially resolved X-ray fluorescence microprobe characterization of the manganese dissolution-deposition mechanism in aqueous Zn/α-MnO_2 batteries. *Energy Environ. Sci.* **2020**, *13* (11), 4322−4333.
(22) Kuai, C.; Liu, L.; Hu, A.; Zhang, Y.; Zhang, Y.; Xia, D.; Nordlund, D.; Sokaras, D.; Decarolis, D.; Gianolio, D.; Xin, H.; Li, L.; Lin, F. Dissolved Fe species enable a cooperative solid-molecular mechanism for the oxygen evolution reaction on NiFe-based catalysts. *Nat. Catal.* **2025**, *8* (6), 523−535.
(23) Lin, F.; Liu, Y.; Yu, X.; Cheng, L.; Singer, A.; Shpyrko, O. G.; Xin, H. L.; Tamura, N.; Tian, C.; Weng, T.-C.; Yang, X.-Q.; Meng, Y. S.; Nordlund, D.; Yang, W.; Doeff, M. M. Synchrotron X-ray Analytical Techniques for Studying Materials Electrochemistry in Rechargeable Batteries. *Chem. Rev.* **2017**, *117* (21), 13123−13186.
(24) Eldesoky, A.; Logan, E. R.; Johnson, M. B.; McFarlane, C. R. M.; Dahn, J. R. Scanning Micro X-ray Fluorescence (μXRF) as an Effective Tool in Quantifying Fe Dissolution in $LiFePO_4$ Cells: Towards a Mechanistic Understanding of Fe Dissolution. *J. Electrochem. Soc.* **2020**, *167* (13), 130539.
(25) Eldesoky, A.; Kowalski, N.; Ni, H.; Logan, E. R.; Zsoldos, E.; Dutta, A.; Zhang, N.; Dahn, J. R. Studying The Impact of Electrolyte, Li Excess, NMC Blending, and Cycling Conditions on The Lifetime and Degradation of LMO/AG Cells Using UHPC Cycling, XRF, and Isothermal Microcalorimetry. *J. Electrochem. Soc.* **2023**, *170* (9), 090530.
(26) Kankanallu, V. R.; Zheng, X.; Leshchev, D.; Zmich, N.; Clark, C.; Lin, C.-H.; Zhong, H.; Ghose, S.; Kiss, A. M.; Nykypanchuk, D.; Stavitski, E.; Takeuchi, E. S.; Marschilok, A. C.; Takeuchi, K. J.; Bai, J.; Ge, M.; Chen-Wiegart, Y.-C. K. Elucidating a dissolution-deposition reaction mechanism by multimodal synchrotron X-ray characterization in aqueous Zn/MnO_2 batteries. *Energy Environ. Sci.* **2023**, *16* (6), 2464−2482.
(27) Zhang, B.; Gao, L.; Hwang, S.; Zhang, C.; Li, T.; Zachman, M. J.; Chang, A.; Liang, J.; Feng, Z.; Cullen, D. A.; Wang, Z.; Li, L.; Wu, G. Constructing Highly Durable Fuel Cell Catalysts Through Integrating Graphitic Shell-Protected Composite Carbon Support with Gaseous Co Deposition-Driven PtCo Intermetallics. *Adv. Mater.* **2026**, *38* (8), No. e2520651.
(28) Michelson, A.; Minevich, B.; Emamy, H.; Huang, X.; Chu, Y. S.; Yan, H.; Gang, O. Three-Dimensional Visualization of Nanoparticle Lattices and Multimaterial Frameworks. *Science* **2022**, *376*, 203−207.
(29) de Jonge, M. D.; Vogt, S. Hard X-ray fluorescence tomography — an emerging tool for structural visualization. *Curr. Opin. Struct. Biol.* **2010**, *20* (5), 606−614.
(30) Lee, P.-T.; Marin, F. S.; Nikitin, V. V.; Antipova, O. A.; Müller, B.; Wang, G. An innovative integration of high-resolution synchrotron x-ray laminography fluorescence imaging. In *Developments in X-Ray Tomography XV*; Müller, B., Wang, G., Eds.; Proc. SPIE, Vol. *13152*; SPIE: Bellingham, WA, 2024; p 1315207. DOI: 10.1117/12.3028127.
(31) Chen, Y.; Zhang, S.; Zhang, W.; Quadrelli, A.; Jarvis, S.; Chen, J.; Lu, H.; Mangayarkarasi, N.; Niu, Y.; Tao, J.; Zhang, L.; Li, J.; Lin, Y.; Huang, Z.; Kolosov, O. Operando nano-mapping of sodium-diglyme co-intercalation and SEI formation in sodium ion batteries' graphene anodes. *Appl. Phys. Rev.* **2024**, *11* (2), 021422.
(32) Zhang, Y.; Katayama, Y.; Tatara, R.; Giordano, L.; Yu, Y.; Fraggedakis, D.; Sun, J. G.; Maglia, F.; Jung, R.; Bazant, M. Z.; Shao-Horn, Y. Revealing electrolyte oxidation via carbonate dehydrogenation on Ni-based oxides in Li-ion batteries by in situ Fourier transform infrared spectroscopy. *Energy Environ. Sci.* **2020**, *13* (1), 183−199.
(33) Guan, L.; Bo, X. Recent advances in surface coating and atomic doping strategies for lithium-ion battery cathodes: implementation approaches and functional mechanisms. *J. Solid State Electrochem.* **2024**, *28* (10), 3517−3532.
(34) Wu, J.; Li, H.; Liu, Y.; Ye, Y.; Yang, Y. Doping and Coating Synergy to Improve the Rate Capability and Cycling Stability of Lithium-Rich Cathode Materials for Lithium-Ion Batteries. *J. Phys. Chem. C* **2022**, *126* (5), 2410−2423.
(35) Bae, J.; Choi, K.; Cheong, J. Y.; Ahn, S.; Cho, S.; Im, S. G.; Kim, I. D. Emerging Surface Engineering Methods for Lithium Metal Anodes: Critical Review Beyond Conventional SEI and Surface Coatings. *Adv. Mater.* **2025**, *37* (38), No. e2501959.
(36) Zhang, Y.; Hu, A.; Xia, D.; Hwang, S.; Sainio, S.; Nordlund, D.; Michel, F. M.; Moore, R. B.; Li, L.; Lin, F. Operando characterization and regulation of metal dissolution and redeposition dynamics near battery electrode surface. *Nat. Nanotechnol.* **2023**, *18* (7), 790−797.
(37) Qian, H.; Ren, H.; Zhang, Y.; He, X.; Li, W.; Wang, J.; Hu, J.; Yang, H.; Sari, H. M. K.; Chen, Y.; Li, X. Surface Doping vs. Bulk Doping of Cathode Materials for Lithium-Ion Batteries:*A Review*. *Electrochem. Energy Rev.* **2022**, *5* (4), 2.
(38) Zhao, C.; Jeong, H.; Hwang, I.; Li, T.; Wang, Y.; Bai, J.; Li, L.; Zhou, S.; Su, C. C.; Xu, W.; Yang, Z.; Almazrouei, M.; Sun, C.-J.; Cheng, L.; Xu, G.-L.; Amine, K. Polysulfide-incompatible additive suppresses spatial reaction heterogeneity of Li-S batteries. *Joule* **2024**, *8* (12), 3397−3411.
(39) Logan, E. R.; Hebecker, H.; Eldesoky, A.; Luscombe, A.; Johnson, M. B.; Dahn, J. R. Performance and Degradation of $LiFePO_4$/Graphite Cells: The Impact of Water Contamination and an Evaluation of Common Electrolyte Additives. *J. Electrochem. Soc.* **2020**, *167* (13), 130543.
(40) Taskovic, T.; Thompson, L. M.; Eldesoky, A.; Lumsden, M. D.; Dahn, J. R. Optimizing Electrolyte Additive Loadings in NMC532/Graphite Cells: Vinylene Carbonate and Ethylene Sulfate. *J. Electrochem. Soc.* **2021**, *168* (1), 010514.
(41) Zhang, Z.; Said, S.; Lovett, A. J.; Jervis, R.; Shearing, P. R.; Brett, D. J. L.; Miller, T. S. The Influence of Cathode Degradation Products on the Anode Interface in Lithium-Ion Batteries. *ACS Nano* **2024**, *18* (13), 9389−9402.
(42) Eldesoky, A.; Bauer, M.; Bond, T.; Kowalski, N.; Corsten, J.; Rathore, D.; Dressler, R.; Dahn, J. R. Long-Term Study on the Impact of Depth of Discharge, C-Rate, Voltage, and Temperature on the Lifetime of Single-Crystal NMC811/Artificial Graphite Pouch Cells. *J. Electrochem. Soc.* **2022**, *169* (10), 100531.
(43) Xia, D.; Tao, L.; Hou, D.; Hu, A.; Sainio, S.; Nordlund, D.; Sun, C.; Xiao, X.; Li, L.; Huang, H.; Lin, F. A Green, Fire-Retarding Ether Solvent for Sustainable High-Voltage Li-Ion Batteries at Standard Salt Concentration. *Adv. Energy Mater.* **2024**, *14* (38), 2400773.
(44) Zhao, M.; Peng, H. J.; Li, B. Q.; Huang, J. Q. Kinetic Promoters for Sulfur Cathodes in Lithium-Sulfur Batteries. *Acc. Chem. Res.* **2024**, *57* (4), 545−557.
(45) Lang, S.; Yu, S. H.; Feng, X.; Krumov, M. R.; Abruna, H. D. Understanding the lithium-sulfur battery redox reactions via operando confocal Raman microscopy. *Nat. Commun.* **2022**, *13* (1), 4811.
(46) Ke, J.; Wang, Z.; Zhu, H.; Chen, M.; Song, R.; Ji, Q.; Liu, D.; Lan, S. Suppression strategies for the polysulfide shuttle effect in electrolyte systems. *Commun. Mater.* **2025**, *6* (1), 237.
(47) Kim, S. J.; Wu, D.; Housel, L. M.; Wu, L.; Takeuchi, K. J.; Marschilok, A. C.; Takeuchi, E. S.; Zhu, Y. Toward the Understanding of the Reaction Mechanism of Zn/MnO_2 Batteries Using Non-alkaline Aqueous Electrolytes. *Chem. Mater.* **2021**, *33* (18), 7283−7289.
(48) He, Y.; Wang, C.; Zhang, R.; Zou, P.; Chen, Z.; Bak, S.-M.; Trask, S. E.; Du, Y.; Lin, R.; Hu, E.; Xin, H. L. A self-healing plastic ceramic electrolyte by an aprotic dynamic polymer network for lithium metal batteries. *Nat. Commun.* **2024**, *15* (1), 10015.
(49) Sun, W.; Wang, F.; Hou, S.; Yang, C.; Fan, X.; Ma, Z.; Gao, T.; Han, F.; Hu, R.; Zhu, M.; Wang, C. Zn/MnO2 Battery Chemistry With H^+ and Zn^{2+} Coinsertion. *J. Am. Chem. Soc.* **2017**, *139* (29), 9775−9778.
(50) Lee, B.; Yoon, C. S.; Lee, H. R.; Chung, K. Y.; Cho, B. W.; Oh, S. H. Electrochemically-induced reversible transition from the tunneled to layered polymorphs of manganese dioxide. *Sci. Rep.* **2014**, *4*, 6066.
(51) Pan, H.; Shao, Y.; Yan, P.; Cheng, Y.; Han, K. S.; Nie, Z.; Wang, C.; Yang, J.; Li, X.; Bhattacharya, P.; Mueller, K. T.; Liu, J. Reversible aqueous zinc/manganese oxide energy storage from conversion reactions. *Nat. Energy* **2016**, *1* (5), 16039.
(52) Kankanallu, V. R.; Zheng, X.; Lo, C.-A.; Kiss, A.; Musterman, E.; Pattammattel, A.; Marschilok, A. C.; Takeuchi, E. S.; Takeuchi, K. J.;

Huang, X.; Ge, M.; Chen-Wiegart, Y.-C. K. Spatial and chemical heterogeneity in aqueous Zn/MnO_2 batteries: role of Zn and Mn containing complexes. *J. Mater. Chem. A* **2025**, *13* (48), 41734−41751.
(53) Li, J.; Chen, S.; Ratner, D.; Blu, T.; Pianetta, P.; Liu, Y. Nanoscale chemical imaging with structured X-ray illumination. *Proc. Natl. Acad. Sci. U.S.A.* **2023**, *120* (49), No. e2314542120.

https://doi.org/10.1021/accountsmr.6c00091
Acc. Mater. Res. 2026, 7, 860−870